Date of publication xxxx 00, 0000, date of current version xxxx 00, 0000.

Digital Object Identifier 10.1109/ACCESS.2017.DOI

Capacity Bounds for Dense Massive MIMO in a Line-of-Sight Propagation Environment

FELIPE A. P. DE FIGUEIREDO[1,2], CLAUDIO F. DIAS[4], EDUARDO R. DE LIMA[3], AND GUSTAVO FRAIDENRAICH[4]

[1]Instituto Nacional de Telecomunicações – INATEL Santa Rita do Sapucaí, MG, Brazil.
[2]Ghent University–imec, IDLab, Department of Information Technology, Ghent, Belgium. (e-mail: felipe.pereira@ugent.be)
[3]Eldorado Research Institute, Campinas, Brazil. (eduardo.lima@eldorado.org.br)
[4]DECOM/FEEC–State University of Campinas (UNICAMP), Campinas Brazil. ([aplnx, gf]@decom.fee.unicamp.br)

Corresponding author: Felipe A. P. de Figueiredo (e-mail: felipe.pereira@ugent.be).

ABSTRACT The use of large-scale antenna arrays grants considerable benefits in energy and spectral efficiency to wireless systems due to spatial resolution and array gain techniques. By assuming a dominant line-of-sight environment in a massive MIMO scenario, we derive analytical expressions for the sum-capacity. Then, we show that convenient simplifications on the sum-capacity expressions are possible when working at low and high SNR regimes. Furthermore, in the case of a high SNR regime, it is demonstrated that the Gamma PDF can approximate the PDF of the instantaneous channel sum-capacity as the number of BS antennas grows. A second important demonstration presented in this work is that a Gamma PDF can also be used to approximate the PDF of the summation of the channel's singular values as the number of devices increases. Finally, it is important to highlight that the presented framework is useful for a massive number of Internet of Things devices as we show that the transmit power of each device can be made inversely proportional to the number of BS antennas.

INDEX TERMS Massive MIMO, channel capacity, dense networks, outage probability.

I. INTRODUCTION

During the past years, we have been witnessing Massive Multiple-Input Multiple-Output (MIMO) becoming an efficient and indispensable sub-6 GHz physical-layer technology for wireless and mobile networks. The embodiment of such technology was vital for the current 5G New Radio (NR) interface [1]. The central concept behind Massive MIMO is the use of a large antenna array deployed at base stations (BS) to simultaneously serve a large number of devices over the same time-frequency resources. In this way, the technique allows exploiting differences among the propagation signatures of the devices in order to perform spatial multiplexing [1]. Even though the Massive MIMO technology looks quite mature, being adopted by new standards, it does not mean an end for research in this subject but just the beginning of unforeseen possibilities [2].

Current requirements for next-generation networks such as high bit rates, very low latency, high energy efficiency, and link robustness are not wholly met even by the current 5G solutions [3]. Thus, there are still several open challenges that need to be addressed by researchers.

One of the approaches used to increase throughput is by increasing the network density, that is, decreasing the size and increasing the number of cells in the same coverage area. As a result, the size of the cells is becoming smaller and smaller, and consequently, it is quite probable that wireless channels will be predominantly line-of-sight (LOS) [4]. Furthermore, the LOS characteristic becomes even more apparent as technology moves to millimeter-wave bands in order to fulfill the requirements for wider bandwidths ($i.e.$, micro and femtocells) [5], [6].

Densification is a natural process for wireless communication networks as the demands for connectivity increases. Thanks to smartphones, tablets, and the internet of things, wireless subscribers are using more network resources with no sign of a decrease in the demand rate. Operators need to add more capacity to their networks to continue handling all the traffic while providing the network speeds those users expect. An arbitrary coverage region can be expected to follow three different degrees of BS densification [2], [7]:

low-density, dense and ultra-dense.

Starting from low-density, the smart farming and rural broadband services provision ($i.e.$, distant areas with low population density) stewards a significant gap in the research body of Massive MIMO nowadays [8], [9]. In the sense of wireless services, it is essential to observe that most economically viable areas for agriculture are the plain terrains with few obstacles [10]. Thus, since the multipath-channel statistics of rural and distant areas are different from those found in urban centers, the wireless channel will likely to be predominantly LOS in such areas [11], [12].

For regions where high value goods are constantly under surveillance, a dense networks is required to communicate with unmanned aerial vehicles (UAVs) or also known as drones [13]. As with the other examples, these communications will probably be LOS-based as well. Additionally, in wireless and cellular communications, the probability that the devices have LoS to the BS is highly probable in many scenarios [14].

Among the approaches and opportunities cited here, the IoT for drones, sensors, automated processes, etc. [15] pose several unsolved research challenges. For example, in the near future, swarms of drones, sensors and actuators will be omnipresent adding up to billions of devices [16]–[18]. In this ultra-dense scenario, these devices will be always moving around the cell at different speeds and positions with a dominant LOS link to the BS. The sum-capacity achieved by a BS serving a massive number of drones, which have a dominant LOS link to the BS and are constantly moving around the cell is still an open issue.

Therefore, in this work, we assume a dominant LOS environment in a massive MIMO scenario with favorable propagation serving a massive number of devices constantly moving within the cell. With this aspect in mind, the objective of this investigation is to find capacity limits concerning the number of devices, number of base station antennas, and SNR. More specifically, the contributions of this work are as follows.

- Derive an analytical expression for the channel sum-capacity.
- Show that the transmit power of each device can be made inversely proportional to the number of BS antennas.
- Find analytical expressions for the upper and lower-bound channel sum-capacities.
- Present expressions for the channel sum-capacity in low and high SNR regimes.
- Demonstrate that the Gamma PDF can approximate the PDF of the instantaneous channel sum-capacity in low and high SNR regimes.
- Demonstrate that a Gamma PDF can also approximate the PDF of the summation of the channel's singular values (also known as total power gain of the channel matrix) as the number of devices increases.

The remaining of this paper is organised as follows: Section II discuss some related works. Section III presents the system model adopted in this work while Section IV discusses aspects of favorable propagation in the current investigated conditions. Section V reviews the concept of favorable propagation. Section VI presents the results with parameters from reference systems. Finally, we close our discussion in the Section VII summarising our conclusions.

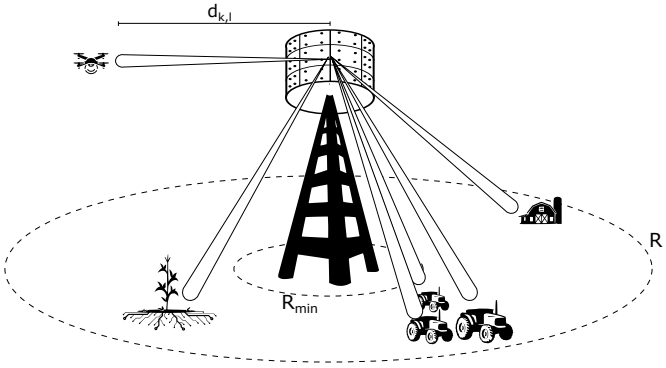

FIGURE 1. Illustration of the adopted system model.

II. RELATED WORK

In [14] the authors analyse the performance of the outage capacity for the uplink of Massive MIMO systems considering a random LoS scenario. The authors of [19] prove that the distribution of the interference term in the expression of the uplink signal-to-interference-plus-noise ratio (SINR) can be approximated as a Beta-mixture when LoS channels and element spacing of half-wavelength are considered. In [20], the authors assess the distribution of the interference and the probability of outage for the downlink of massive MIMO systems adopting MRC precoding in rich multi-path scenarios. In [21], the authors demonstrate that in massive MIMO systems the LoS channels are asymptotically orthogonal as the number of antennas increases. They also demonstrate that when a finite number of antennas is considered, the channels will not be orthogonal. The impact of antenna element spacing on the capacity of fixed point-to-point massive MIMO systems considering LoS channels was evaluated in [22].

III. SYSTEM MODEL

Here we present the channel model adopted in [1]. We assume a channel model with only free-space non-fading ($i.e.$, pure) LOS propagation between the BS and the devices and that the BS is equipped with an uniform linear array (ULA) with the M antenna elements spaced of $\lambda/2$, where λ is the signal's wavelength. There are K single-antenna devices deployed randomly within the cell that simultaneously transmit data towards the BS through the same time-frequency resources. Additionally, we also consider that all the K devices being served by the BS are located in the far-field of the antenna array at the angle θ_k as measured relative to the array bore-sight [1]. Therefore,

$$\mathbf{G} = \mathbf{HBD}^{1/2}, \tag{1}$$

where the elements of the matrix $\mathbf{H}$ are defined as $h_{mk} = e^{-j(m-1)\sin(\theta_k)}$, m is the antenna index, k is the device index, θ_k models the devices' locations and is uniformly distributed in the interval $[-\pi, \pi]$, the elements of the diagonal matrix $\mathbf{B}$ are defined as $b_k = e^{j\phi_k}$, ϕ_k is a uniformly distributed random variable defined in the range $[-\pi,\ \pi]$ that models the phase shift associated with a random range between the array and the k-th device, and the elements of the diagonal matrix $\mathbf{D}$ that defined as $d_k = \beta_k$ are the large-scale fading coefficients [1].

The free space path-loss coefficients, β_{km}, is modeled as described in [23],

$$\beta_{km} = \frac{\eta}{d_{k,m}^2}, \tag{2}$$

where η is a constant equal to $\left(\frac{\lambda}{4\pi}\right)^2$ [24], $d_{k,m}$ is the distance between the m-th BS antenna and the k-th terminal's antenna, and the path-loss exponent is equal to 2, which is the value used for free-space propagation. As the distance between the k-th device and the antenna array is $d_{k,m} \gg \lambda$, then $d_{k,m} \approx d_k$, and consequently $\beta_{km} \approx \beta_k$, *i.e.*, β_{km} does not depend on the antenna index as the distance between the k-th device and the BS is much greater than the distance between the antennas. We consider that d_k is an uniformly distributed random variable distributed in the interval $[R_{\text{min}}, R]$, where R_{min} is the minimum distance a device can be from the BS and R is the cell radius. The adopted system model is depicted in Figure 1.

IV. CHANNEL SUM-CAPACITY IN LOS AND FAVORABLE PROPAGATION CONDITIONS

The distance between the device's antennas and the BS's antennas is not static as the devices are always moving within the cell (*e.g.*, drones, cars, etc.). Therefore, the distance has to be treated as a random variable, resulting in a different channel realization for every time instant. As it is known [1], the instantaneous sum-capacity is not a meaningful performance metric under such random conditions. Here, we are interested in the capacity performance averaged over all different positions a device might be within the cell. Therefore, in order to assess the performance in this scenario, we need to employ the notion of ergodic capacity, which results in the following uplink sum link capacity [25]

$$\begin{aligned} C &= \mathbb{E}\left[\log_2|\mathbf{I}_M + \rho\mathbf{G}\mathbf{G}^H|\right] \\ &= \mathbb{E}\left[\log_2|\mathbf{I}_K + \rho\mathbf{G}^H\mathbf{G}|\right]. \end{aligned} \tag{3}$$

where ρ is the average signal-to-interference ratio (SNR), also known as average transmitted power of each device, and the expectation is taken over the joint distribution of all possible positions of the devices. As the additive white noise is assumed to have mean and variance equal to 0 and 1 respectively, therefore, ρ has, consequently, the interpretation of normalized transmit SNR and is therefore dimensionless [26]. It is important to highlight that the expectation in (3) is taken in relation with devices' channels, more specifically in relation with their positions within the cell (*i.e.*, distances and angles of arrival), which are considered as random variables. The second line of (3) is found by applying the Sylvester's determinant theorem. Furthermore, we assume that the base station has perfect knowledge of the channel matrix $\mathbf{G}$. The rationale behind the assumption of perfect knowledge of the channel matrix is that the results obtained with this assumption are readily comprehended and they bound the performance of massive MIMO systems.

Finding the exact ergodic capacity given by (3) is a quite complex task that involves finding the distribution of the eigenvalues of $\mathbf{G}^H\mathbf{G}$ [27]. In this work, as we will show next, we are concerned with finding the sum-capacity considering a Massive MIMO scenario and asymptotically favorable propagation [1]. In asymptotically favorable propagation scenarios, the channel vectors of different users become mutually orthogonal as the number of antennas, M, increases, *i.e.*,

$$\frac{\mathbf{g}_i^H\mathbf{g}_j}{M} \overset{M\to\infty}{\to} 0, \quad \forall\ i \neq j. \tag{4}$$

The environment is said to offer asymptotically favorable propagation when (4) is satisfied. The mutual orthogonality offered by environments exhibiting the asymptotic favorable propagation condition is the most beneficial situation from the perspective of sum-capacity maximization. Then, the sum-capacity in (3) can be re-expressed as

$$\begin{aligned} C &= \mathbb{E}\left[\log_2|\mathbf{I}_K + \rho\mathbf{G}^H\mathbf{G}|\right] \\ &\leq \mathbb{E}\left[\log_2\left(\prod_{k=1}^{K}\left[\mathbf{I}_K + \rho\mathbf{G}^H\mathbf{G}\right]_{k,k}\right)\right] \\ &= \mathbb{E}\left[\sum_{k=1}^{K}\log_2\left(\left[\mathbf{I}_K + \rho\mathbf{G}^H\mathbf{G}\right]_{k,k}\right)\right] \\ &= \mathbb{E}\left[\sum_{k=1}^{K}\log_2\left(1 + \rho\|\mathbf{g}_k\|^2\right)\right]. \end{aligned} \tag{5}$$

The inequality in the second line of (5) is found applying the Hadamard inequality and assuming that $\|\mathbf{g}_k\|^2, \forall k$ is known, where $\mathbf{g}_k, \forall k$, are the columns of the channel matrix $\mathbf{G}$. As will be shown latter, this bound will be proven to be very tight. The equality in the second line of (5) holds if and only if $\mathbf{G}^H\mathbf{G}$ is a diagonal matrix (*i.e.*, the channel matrix $\mathbf{G}$ has mutually orthogonal columns) that must satisfy [28],

$$\mathbf{g}_i^H\mathbf{g}_j = \begin{cases} 0, & i,j = 1,\ldots,K, \text{ for } i \neq j \\ \|\mathbf{g}_k\|^2 = M\beta_k, & k = 1,\ldots,K, \text{ for } i = j, \end{cases} \tag{6}$$

which is the case when the channel exhibits favorable propagation [29]. The equality $\|\mathbf{g}_k\|^2 = M\beta_k$ is detailed in Appendix A.

Given the assumption of channels exhibiting asymptotically favorable propagation, we know from [1] that the spatial signature vectors, denoted by $e^{j\phi_k}\mathbf{h}_k$, become asymptotically mutually orthogonal and consequently, it can be shown that

$$\frac{\mathbf{B}^H\mathbf{H}^H\mathbf{H}\mathbf{B}}{M} \overset{M\to\infty}{\approx} \mathbf{I}_K, \tag{7}$$

and therefore,

$$\frac{\mathbf{G}^H\mathbf{G}}{M} = \mathbf{D}^{1/2}\frac{\mathbf{B}^H\mathbf{H}^H\mathbf{H}\mathbf{B}}{M}\mathbf{D}^{1/2} \overset{M\to\infty}{\approx} \mathbf{D}, \tag{8}$$

hence, the results presented in this work hold for any type of antenna array, *i.e.*., ULA and uniform rectangular array (URA), as in the asymptotic regime (8) will always tend to the matrix containing the large-scale fading coefficients.

Now using $\|\mathbf{g}_k\|^2 = M\beta_k$ and $\beta_k = \frac{\eta}{d_k^2}$ in the last line of (5), the sum-capacity upper bound can be re-written as

$$\begin{aligned} C &= \sum_{k=1}^{K}\mathbb{E}\left[\log_2\left(1+\frac{\rho M\eta}{d_k^2}\right)\right] \\ &= K\mathbb{E}\left[\log_2\left(1+\frac{\rho M\eta}{d_k^2}\right)\right], \end{aligned} \tag{9}$$

where the last equality is due to the fact that d_k is an i.i.d. random variable for all k.

Next, considering $z = \frac{1}{d_k^2}$ as a random variable denoted by Z with probability density function (PDF) given by

$$f_Z(z) = \frac{1}{2(R-R_{min})z\sqrt{z}}, \quad \frac{1}{R^2} \le z \le \frac{1}{R_{min}^2}, \tag{10}$$

then, (9) can be re-expressed as

$$\begin{aligned} C &= K\mathbb{E}\left[\log_2\left(1+\frac{\rho M\eta}{d_k^2}\right)\right] \\ &= K\mathbb{E}\left[\log_2\left(1+\rho M\eta z\right)\right] \\ &= \frac{K}{2(R-R_{min})}\int_{1/R^2}^{1/R_{min}^2}\log_2(1+\rho M\eta z)\frac{1}{z\sqrt{z}}dz, \end{aligned} \tag{11}$$

where the proof of (10) is given in Appendix B. Next, solving (11) with an integral solver [30], we find an exact closed-form expression given in (12) for the capacity when the channel offers favorable propagation.

Remark 1. *After analyzing* (12)*, we see that if we make the transmit power of each device equal to P/M^α, where $\alpha > 1$, then the sum-capacity, C, will go to zero as $M \to \infty$. When $\alpha < 1$ the sum-capacity grows without bound as $M \to \infty$. This means that $1/M$ (i.e., $\alpha = 1$) is the fastest rate at which we can decrease the transmit power of each device and still have a fixed capacity as $M \to \infty$.*

Remark 1 clearly shows that as M grows without bound, the transmit power of each device can be reduced proportionally to $1/M$ and that the spectral efficiency increases by a factor of K, meaning that the BS can simultaneously serve K devices over the same time-frequency resources. This reduction of the transmit power per device is very important to power-constrained devices such as IoT devices.

A. APPROXIMATED DISTRIBUTION OF THE TOTAL POWER GAIN

The sum-capacity given by the first line of (5) can be expressed in terms of the singular values $\{\lambda_k\}$ of the channel matrix $\mathbf{G}$ and, therefore, if $\lambda_1 \ge \lambda_2 \ge \cdots \lambda_K$ are the random ordered singular values of $\mathbf{G}$, then (5) can be re-written as [1]

$$C = \mathbb{E}\left[\sum_{k=1}^{K}\log_2\left(1+\rho\lambda_k^2\right)\right]. \tag{14}$$

By comparing (5) and (14), it is possible to conclude that

$$\lambda_k^2 = \|g_k\|^2 = M\beta_k. \tag{15}$$

The singular values represent the channel gains of the parallel channels after Singular Value Decomposition (SVD) of the system [25]. Next we present the squared Frobenius norm of $\mathbf{G}$ when the environment offers favorable propagation, and consequently, $\mathbf{G}$ is full rank

$$\|\mathbf{G}\|_F^2 = \sum_{m=1}^{M}\sum_{k=1}^{K}|g_{mk}|^2 = \mathrm{Tr}(\mathbf{G}^H\mathbf{G}) = \sum_{k=1}^{K}\lambda_k^2. \tag{16}$$

The last term of (16) can be interpreted as the total power gain of the channel matrix if one spreads the energy equally between all the antennas [25]. Therefore, comparing (15) and (16), we clearly see that the singular values have the same distribution as the free space path-loss coefficients, $\beta_k, \forall k$. The summation of the K free space path-loss coefficients, is a random variable that can be approximated by the Gamma distribution as showed in Appendix D.

B. A LOWER-BOUND FOR THE CAPACITY

First we define the following Jensen's Inequality [31]

$$\mathbb{E}\left[\log_2(1+z)\right] \ge \log_2\left(1+\frac{1}{\mathbb{E}\left[\frac{1}{z}\right]}\right), \tag{17}$$

where $z = \frac{1}{u}$ for $z > 0$. Therefore, (9) can be re-written as

$$\begin{aligned} C &= K\mathbb{E}\left[\log_2\left(1+\frac{\rho M\eta}{d_k^2}\right)\right] \\ &\ge K\log_2\left(1+\frac{\rho M\eta}{\mathbb{E}\left[d_k^2\right]}\right). \end{aligned} \tag{18}$$

Remembering that $f_d(r) = \frac{1}{R-R_{\min}}$, $R_{\min} \le r \le R$, then

$$\mathbb{E}\left[d_k^2\right] = \frac{R^3-R_{min}^3}{3(R-R_{min})}. \tag{19}$$

For proof of (19), see Appendix C. Therefore, (18) can be re-expressed as

$$C \ge K\log_2\left(1+\frac{3\rho M\eta(R-R_{min})}{R^3-R_{min}^3}\right). \tag{20}$$

C. AN UPPER-BOUND FOR THE CAPACITY

Again, we can use the Jensen's Inequality as

$$\mathbb{E}\left[\log_2(1+z)\right] \le \log_2\left(1+\mathbb{E}\left[z\right]\right), \tag{21}$$

for $z > 0$. Therefore, (9) can be re-written as

$$\begin{aligned} C &= K\mathbb{E}\left[\log_2\left(1+\frac{\rho M\eta}{d_k^2}\right)\right] \\ &\le K\log_2\left(1+\rho M\eta\mathbb{E}\left[\frac{1}{d_k^2}\right]\right). \end{aligned} \tag{22}$$

$$C = \frac{K}{(R-R_{min})} \frac{2\sqrt{\rho M\eta}\left(\tan^{-1}\left(\sqrt{\frac{\rho M\eta}{R_{min}^2}}\right) - \tan^{-1}\left(\sqrt{\frac{\rho M\eta}{R^2}}\right)\right) + R\log\left(\frac{\rho M\eta}{R^2}+1\right) - R_{min}\log\left(\frac{\rho M\eta}{R_{min}^2}+1\right)}{\log(2)}. \quad (12)$$

$$C \approx \frac{K}{(R-R_{min})} \frac{\log(\rho M\eta)(R-R_{min}) + 2\left[R - R_{min} - R\log(R) + R_{min}\log(R_{min})\right]}{\log(2)}. \quad (13)$$

Remembering that $f_d(r) = \frac{1}{R-R_{\text{min}}}$, $R_{\text{min}} \leq r \leq R$, then

$$\mathbb{E}\left[\frac{1}{d_k^2}\right] = \frac{1}{RR_{min}}. \quad (23)$$

For proof of (23), see Appendix C. Therefore, (22) can be re-expressed as

$$C \leq K\log_2\left(1+\frac{\rho M\eta}{RR_{min}}\right). \quad (24)$$

D. LOW SNR REGIME

For the low SNR regime, we have the following approximation: $\log_2(1+x) \approx x\log_2(e)$, when $x \ll 1$, then (9) can be expressed as

$$\begin{aligned} C &\approx K\mathbb{E}\left[\frac{\rho M\eta}{d_k^2}\log_2(e)\right] \\ &= K\rho M\eta\log_2(e)\,\mathbb{E}\left[\frac{1}{d_k^2}\right] \\ &= \frac{K\rho M\eta\log_2(e)}{RR_{min}}. \end{aligned} \quad (25)$$

In (25), we see that the sum-capacity linearly increases with the average SNR, ρ, and/or with the number of antennas, M.

E. HIGH SNR REGIME

For the high SNR regime, we have the following approximation: $\log_2(1+x) \approx \log_2(x)$, when $x \gg 1$, then (9) can be expressed as

$$\begin{aligned} C &\approx K\mathbb{E}\left[\log_2\left(\frac{\rho M\eta}{d_k^2}\right)\right] \\ &= \frac{K}{2(R-R_{min})}\int_{1/R^2}^{1/R_{min}^2}\log_2(\rho M\eta z)\frac{1}{z\sqrt{z}}dz, \end{aligned} \quad (26)$$

where $z = \frac{1}{d_k^2}$. Solving (26) with an integral solver [30], we find an exact closed-form expression for the capacity when the channel offers favorable propagation in the high SNR regime. The exact closed-form expression for the approximated sum-capacity in (26) is given by (13).

In (13), differently from (25), we see that the sum-capacity logarithmically increases with the average SNR, ρ, and/or with the number of antennas, M. Therefore, in the high SNR regime, an increase in the transmit power and/or in the number of antennas, M, is much less impressive than in the low SNR regime case.

F. INSTANTANEOUS SUM-CAPACITY PDF IN LOW SNR REGIME AND FAVORABLE PROPAGATION CONDITION

The instantaneous sum-capacity in low SNR regime and favorable propagation condition is given by

$$\begin{aligned} C_{\text{inst.}} &= \sum_{k=1}^{K}\log_2\left(1+\frac{\rho M\eta}{d_k^2}\right) \\ &\overset{\frac{\rho M\eta}{d_k^2}\ll 1}{\approx} \rho M\eta\log_2(e)\sum_{k=1}^{K}\frac{1}{d_k^2}, \end{aligned} \quad (27)$$

which is a random variable that depends on the distance of the k-th device to the BS, denoted by d_k.

Lemma 1. *By empirically comparing the normalised histogram of the random variable given by* (27) *against the theoretical PDF of a Gamma random variable we notice that as K increases that $C_{inst.}$ can be approximated by the Gamma PDF with parameters κ and θ given by*

$$\kappa = \frac{3KRR_{min}}{(R-R_{min})^2}, \quad (28)$$

$$\theta = \frac{\rho M\eta\log_2(e)(R-R_{min})^2}{3R^2R_{min}^2}. \quad (29)$$

This comparison is shown in section VI. The parameters κ and θ are found following the same rationale used in Appendix D.

G. INSTANTANEOUS SUM-CAPACITY PDF IN HIGH SNR REGIME AND FAVORABLE PROPAGATION CONDITION

The instantaneous sum-capacity in high SNR regime and favorable propagation condition is given by

$$\begin{aligned} C_{\text{inst.}} &= \sum_{k=1}^{K}\log_2\left(1+\frac{\rho M\eta}{d_k^2}\right) \\ &\overset{\frac{\rho M\eta}{d_k^2}\gg 1}{\approx} \sum_{k=1}^{K}\log_2\left(\frac{\rho M\eta}{d_k^2}\right), \end{aligned} \quad (30)$$

which is a random variable that depends on the distance of the k-th device to the BS, denoted by d_k.

Lemma 2. *By empirically comparing the normalised histogram of the random variable given by* (30) *against the theoretical PDF of a Gamma random variable we notice that as M increases that $C_{inst.}$ can be approximated by the Gamma PDF with parameters κ and θ given by* (33) *and* (34)*, respectively, where $a = \log(\rho M\eta)$, $b = \log\left(\frac{\rho M\eta}{R_{min}^2}\right)$,*

$c = \log\left(\frac{\rho M \eta}{R^2}\right)$, $d = \log\left(\frac{1}{R_{min}^2}\right)$, *and* $e = \log\left(\frac{1}{R^2}\right)$. *This comparison is shown in section VI. The parameters* κ *and* θ *are found as described in Appendix E.*

H. OUTAGE PROBABILITY

Therefore, based on the knowledge of the approximated PDFs, it is possible to use the Gamma's CDF as a way to analyse the outage probability, C_{out}, in low and high SNR regimes. Results comparing the PDF and CDF of the actual random variable and those of a Gamma random variable are presented and discussed in section VI. Outage probability is the probability that a certain sum-capacity cannot be reached and is defined as

$$P_{\text{out}} = \Pr\{C_{\text{inst.}} < C_{\text{out}}\} \quad (31)$$

$$\overset{M \to \infty}{\approx} \frac{1}{\Gamma(\kappa)} \gamma\left(\kappa, \frac{C_{\text{out}}}{\theta}\right), \quad (32)$$

where $\Gamma(.)$ is the gamma function, $\gamma(.,.)$ is the incomplete gamma function, and κ and θ are given by (33) and (34), respectively.

V. AVERAGE DISTANCE FROM FAVORABLE PROPAGATION

The favorable propagation is a important metric which is defined as mutual orthogonality among the vector-valued channels to the terminals [21]. The measure is one of the key properties of the radio channel that is exploited in Massive MIMO. From [21], we can further characterize favorable propagation as

$$\Delta_C = \frac{K\mathbb{E}\left[\log_2(1+\rho M \beta_k)\right] - \mathbb{E}\left[\log_2|I_K + \rho \mathbf{G}^H \mathbf{G}|\right]}{\mathbb{E}\left[\log_2|I_K + \rho \mathbf{G}^H \mathbf{G}|\right]}. \quad (35)$$

As can be seen from (35), when $\Delta_C = 0$, the channel offers favorable propagation. The measure defined in (35) is an extension of the one presented in [1] for the ergodic capacity case assumed in this work.

VI. SIMULATION RESULTS AND DISCUSSION

In this section we present the results of several simulations that were designed to assess the findings we have reported in this work. All results presented here have the following simulation setup parameters $R = 100$ [m], $R_{min} = 10$ [m], and $\lambda = 0.375$ [m], which is equivalent to a carrier frequency of 800 MHz.

Figure 2 has the following simulation setup parameters $K = 10$ and $\rho = 50$ [dB]. As can be seen, the simulated capacity is within the lower and upper bound ranges as expected. It is also possible to see that the simulated and analytical capacities in favorable propagation match each other, showing that the derived analytical closed-form is tight for the favorable propagation case. Moreover, the simulated capacity asymptotically approaches the capacity in favorable propagation as the number of antennas, M, grows, proving that favorable propagation is asymptotically achieved as M grows. It is also important to highlight that the analytical capacity in favorable propagation, given by (12), provides a good approximation for the capacity. For example, for $M = 100$ the simulated capacity is equal to 23.59 bits/s/Hz and the analytical capacity in favorable propagation is equal to 24.44 bits/s/Hz.

Figure 2 also presents on the right x-axis the average distance from favorable propagation as defined in (35). As can be noticed, the average distance asymptotically decreases as the number of antennas grows, starting at 0.14 for $M = 10$ and decreasing to 0.0049 for $M = 1000$. This result is another indication that favorable propagation is asymptotically achieved as M grows.

Figure 3 compares the sum-capacity over the variation of the average SNR, ρ, for the same simulation parameters used for the results in Figure 2 and M constant and equal to 300 antennas. As expected, the sum-capacity, simulated and analytical, stay within the lower and upper capacity bounds. For low SNR values the sum-capacity is closer to the upper bound and as the SNR increases, we see that both lower and upper bounds converge to the sum-capacity.

In Figure 4 we present the results of the sum-capacity for low and high SNR regimes in favorable propagation condition versus the average signal-to-interference ratio, ρ, with M constant and equal to 300 antennas. As can be seen, (25) and (13) represent the sum-capacity fairly well for the low and high SNR regimes, respectively. In the upper part of the figure, we show the sum-capacity for the low SNR regime and it is possible to see that the approximated expression given by (25) closely follows the sum-capacity until around 30 [dB]. In the lower part of the figure, we show the sum-capacity for the high SNR regime and we also see that the approximated expression given by (13) closely follows the sum-capacity for SNR values greater than 40 [dB]. The figure also shows that the sum-capacity grows linearly and logarithmically with the average SNR for the low and high SNR regimes, respectively, confirming what was discussed in subsections IV-D and IV-E

Figure 5 shows how the spectral efficiency behaves as $\rho = P/M^{\alpha}$, where $\alpha = 1/2, 1$ and $3/2$, respectively. The following simulation setup parameters were used: $K = 10$ and $P = 50$ [dB]. As expected and stated in Remark 1, when $\alpha = 1$ and M increases, the capacity becomes constant no matter the number of antennas. However, when $\alpha = 1/2$ the capacity grows logarithmically fast with M when $M \to \infty$ and tends to zero when $\alpha = 3/2$ and $M \to \infty$. These results attest that the transmit power of each device can be reduced proportionally to M.

In Figure 6 we show the required transmit power per device that is needed to achieve fixed capacities of 1 and 2 bits/s/Hz respectively. As expected and predicted by Remark 1, the transmit power can be reduced by approximately 3 [dB] by doubling the number of antennas, M, for both cases, *i.e.*, 1 and 2 bits/s/Hz.

Figure 7 shows the comparison between the normalized histogram of the random variable Z, where Z is defined in Lemma 3, and the Gamma PDF for number of devices equal

$$\kappa = \frac{\frac{K}{(R-R_{\min})}\left(\frac{b+2}{R}-\frac{c+2}{R_{\min}}\right)^2}{\frac{1}{RR_{\min}}\left(\frac{2e(a+2)+e^2+a(a+4)+8}{R_{\min}}-\frac{2d(a+2)+d^2+a(a+4)+8}{R}\right)-\frac{1}{(R-R_{\min})}\left(\frac{b+2}{R}-\frac{c+2}{R_{\min}}\right)^2}. \tag{33}$$

$$\theta = \frac{\frac{RR_{\min}}{(R-R_{\min})}\left(\frac{b+2}{R}-\frac{c+2}{R_{\min}}\right)^2-\frac{2e(a+2)+e^2+a(a+4)+8}{R_{\min}}+\frac{2d(a+2)+d^2+a(a+4)+8}{R}}{\log(2)\left(\frac{b+2}{R}-\frac{c+2}{R_{\min}}\right)}. \tag{34}$$

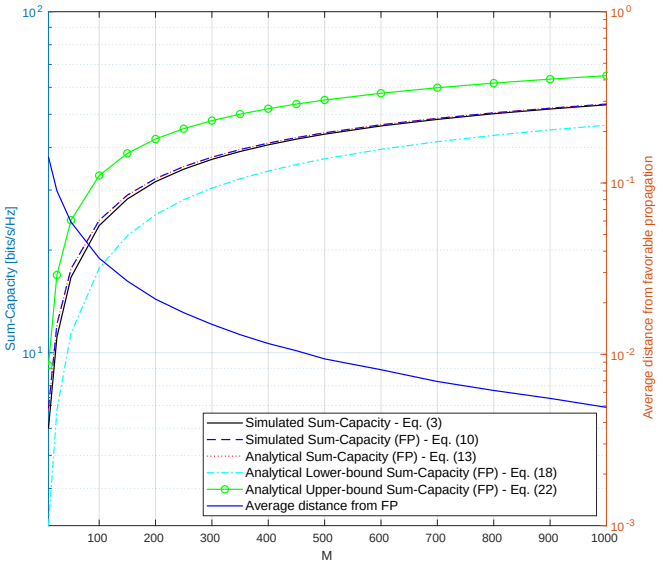

FIGURE 2. Simulation considering $K = 10$, $\rho = 50$ [dB], $R = 100$ [m], $R_{min} = 10$ [m], and $\lambda = 0.375$ [m].

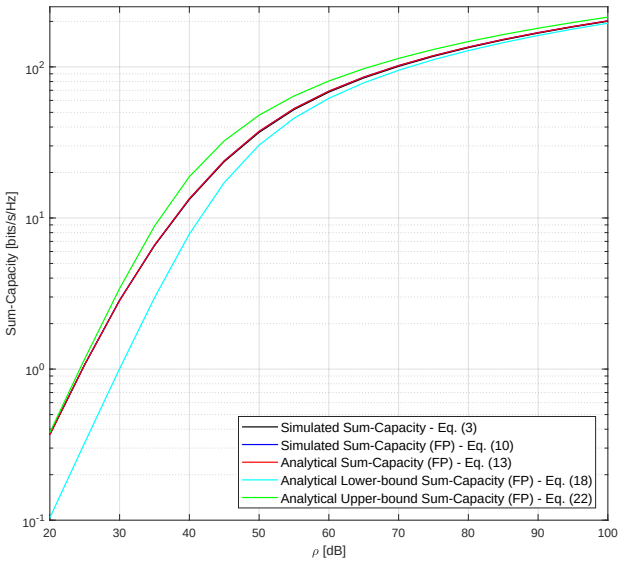

FIGURE 3. Simulated and analytical sum-capacity considering $M = 300$.

to $K = 10$, 20, and 50 respectively. These results were also obtained with the following simulation setup parameters $M = 100$ and $\rho = 50$ [dB]. The histogram, showed in blue, is the histogram of the random variable $Z = \sum_{k=1}^{K} M\beta_k$. As can be seen, the histogram approaches the Gamma PDF as the number of devices increases.

Figure 8 comparison of the instantaneous sum-capacity in high SNR regime and favorable propagation condition and its approximation with the Gamma PDF. This comparison was obtained with the following parameters $K = 10$ and $\rho = 60$ [dB]. As can be seen, for high SNR, the Gamma PDF fits the PDF of the instantaneous sum-capacity random variable as the number of antennas grows.

Figure 9 presents the comparison between the approximated and simulated outage probabilities in the high SNR regime and favorable propagation condition. The simulation parameters are the same used for generating the results in Figure 8. As can be also seen, for high SNR, the Gamma CDF fits the simulated outage probability of the instantaneous sum-capacity random variable as the number of antennas grows.

Figure 10 comparison of the instantaneous sum-capacity in low SNR regime and favorable propagation condition and its

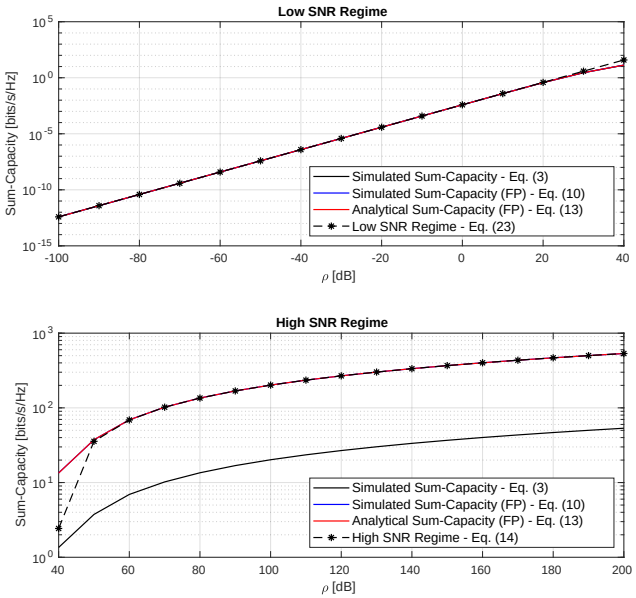

FIGURE 4. Sum-capacity for low and high SNR regimes versus average signal-to-interference ratio, ρ.

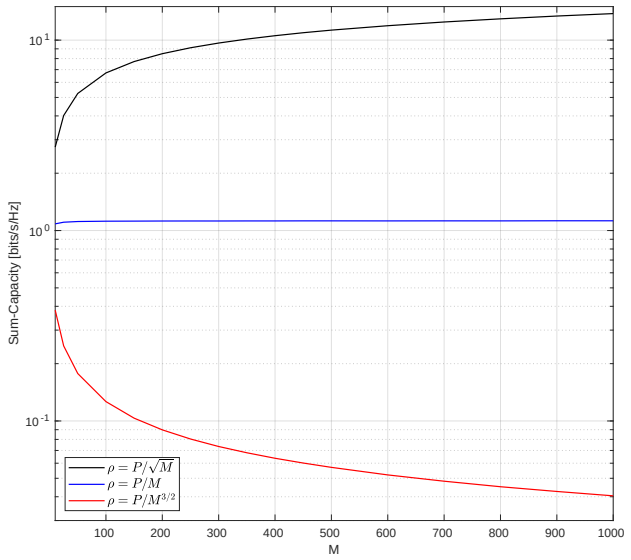

FIGURE 5. Demonstration of the power scaling law for different α values.

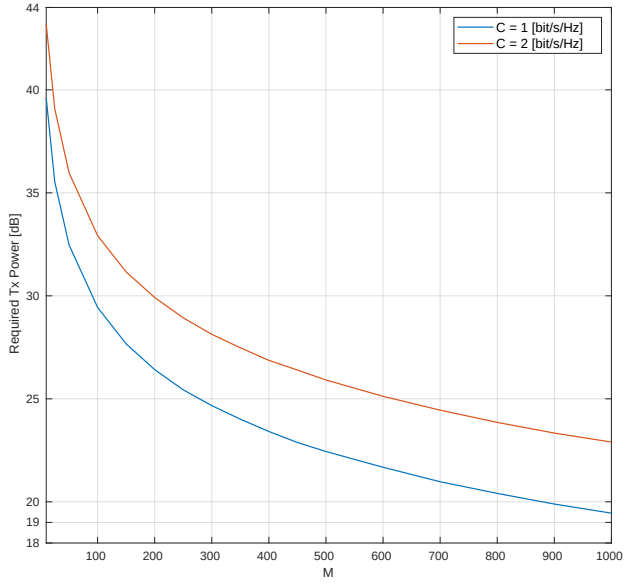

FIGURE 6. Required transmit power to achieve 1 and 2 bits/s/Hz as a function of the number of antennas.

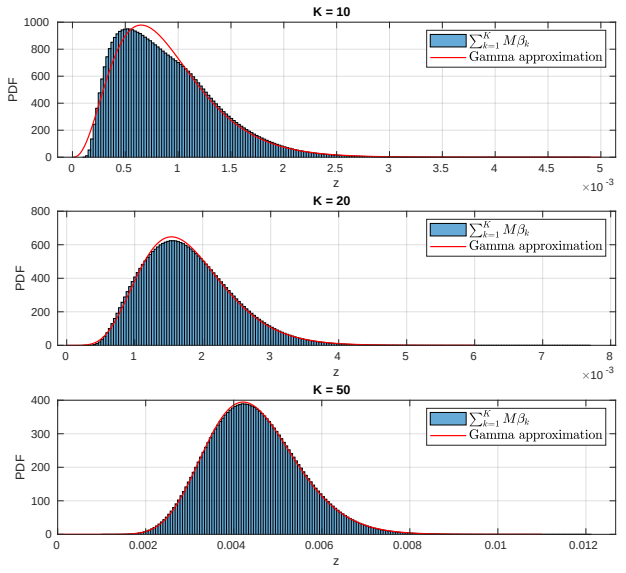

FIGURE 7. Gamma PDF for number of devices equal to $K = 10$, 20, and 50 respectively.

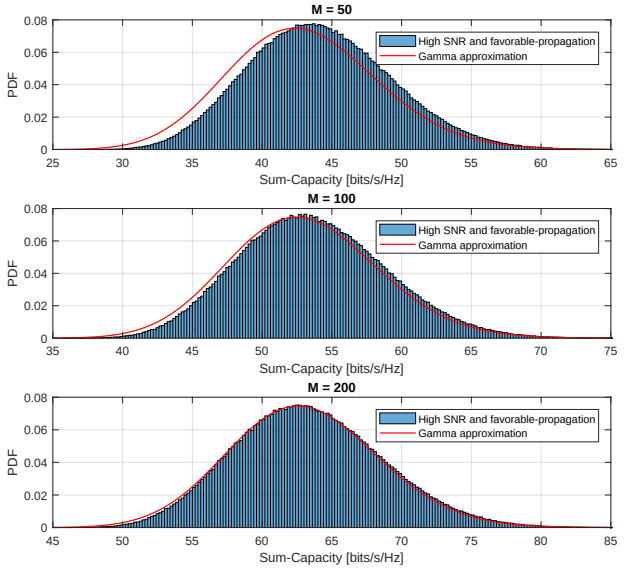

FIGURE 8. Comparison of the approximated PDF for the instantaneous sum-capacity in high SNR regime and favorable propagation condition.

approximation with the Gamma PDF. This comparison was obtained with the following parameters $M = 100$ and $\rho = 0$ [dB]. As can be seen, for low SNR, the Gamma PDF fits the PDF of the instantaneous sum-capacity random variable as the number of devices simultaneously served through the same time-frequency resources grows.

Figure 11 presents the comparison between the approximated and simulated outage probabilities in the low SNR regime and favorable propagation condition. This comparison was obtained with the following parameters $M = 300$ and $\rho = 0$ [dB]. As can be also seen, for low SNR, the Gamma CDF fits the simulated outage probability of the instantaneous sum-capacity random variable as the number of served devices grows.

VII. CONCLUSIONS

In this work, we investigated ways to find capacity limits concerning the number of users, number of BS antennas, and SNR. By assuming a dominant LOS environment in a massive MIMO scenario, it was possible to derive analytical expressions for the channel capacity. Convenient simplifications on expressions were possible working at low and high SNR regimes. Furthermore, it is demonstrated that the Gamma PDF can approximate the PDF of the instantaneous channel sum-capacity as the number of antennas grows for both cases of low and high SNR regimes. A second important demonstration is that a Gamma PDF can also approximate the PDF of the summation of the channel's singular values as

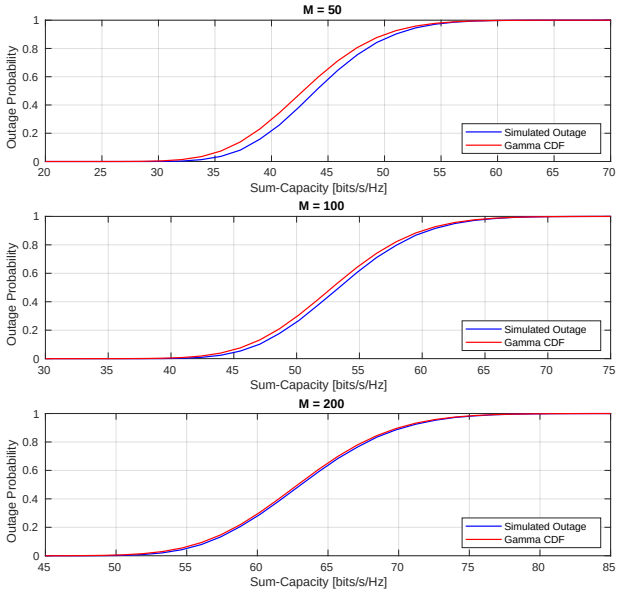

FIGURE 9. Comparison between the approximated and simulated outage probabilities in high SNR regime and favorable propagation condition.

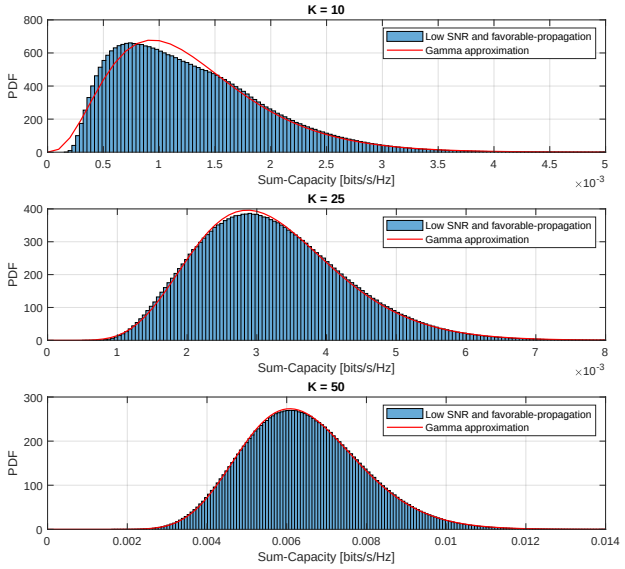

FIGURE 10. Comparison of the approximated PDF for the instantaneous sum-capacity in low SNR regime and favorable propagation condition.

the number of devices increases. Finally, the utility of such a framework is useful for a massive number of IoT devices as we show that the transmit power of each device can be made inversely proportional to the number of BS antennas.

.

APPENDIX A DERIVATION OF $\|\mathbf{g}_K\|^2 = M\beta_K$

From (1), we can write each element $g_{k,m}$ of $\mathbf{g}_k$ as

$$g_{k,m} = \sqrt{\beta_k} e^{j\phi_k} e^{-j(m-1)\sin(\theta_k)}. \tag{36}$$

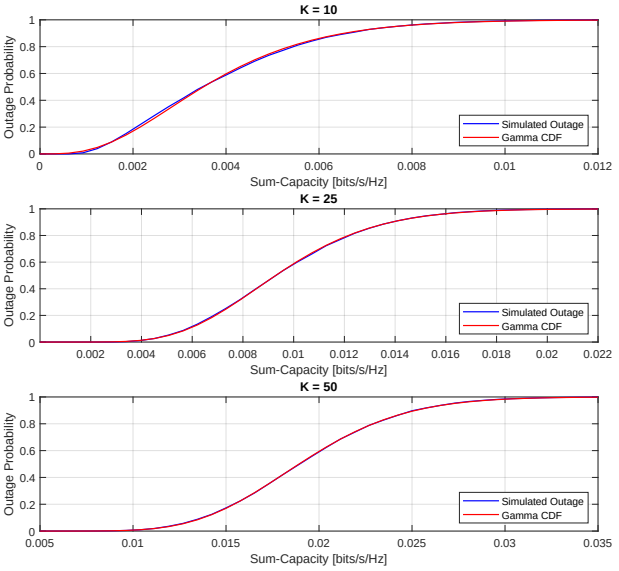

FIGURE 11. Comparison between the approximated and simulated outage probabilities in low SNR regime and favorable propagation condition.

Therefore, using the very definition of the product of two matrices [32], we have

$$\begin{aligned}\|\mathbf{g}_k\|^2 &= \sum_{m=1}^{M} \left| \sqrt{\beta_k} e^{j\phi_k} e^{-j(m-1)\sin(\theta_k)} \right|^2 \\ &= \sum_{m=1}^{M} \left| \sqrt{\beta_k} \right|^2 \left| e^{j\phi_k} \right|^2 \left| e^{-j(m-1)\sin(\theta_k)} \right|^2,\end{aligned} \tag{37}$$

where $\left| e^{j\phi_k} \right|^2 = \left| e^{-j(m-1)\sin(\theta_k)} \right|^2 = 1$ and $\left| \sqrt{\beta_k} \right|^2 = \beta_k$, therefore

$$\|\mathbf{g}_k\|^2 = \sum_{m=1}^{M} \beta_k = M\beta_k. \tag{38}$$

APPENDIX B DERIVATION OF THE PDF OF THE DISTANCE RANDOM VARIABLE

Given that the PDF of Y is defined as

$$f_Y(y) = \frac{1}{R - R_{min}}, \quad R_{min} \leq y \leq R, \tag{39}$$

and the strictly monotonic differentiable function $Z = g(Y) = 1/Y^2$, then the PDF of Z is given by

$$f_Z(z) = \frac{f_Y(g^{-1}(Z))}{|g'(Y)|}, \tag{40}$$

where $g'(Y) = -2/Y^3$ and $g^{-1}(Z) = 1/\sqrt{Z}$. Therefore,

$$\begin{aligned} f_Z(z) &= \frac{f_Y(g^{-1}(Z))}{|g'(Y)|} = \frac{\frac{1}{R-R_{min}}}{\left|\frac{-2}{y^3}\right|} \\ &= \frac{1}{2(R - R_{min})z\sqrt{z}}, \end{aligned} \tag{41}$$

where in the last equality we used the fact that $y = 1/\sqrt{z}$.

APPENDIX C USEFUL RESULTS

A. CALCULATION OF $\mathbb{E}\left[d_k^2\right]$

$$\mathbb{E}\left[d_k^2\right] = \int_{R_{\min}}^{R} r^2 f_d(r) dr = \int_{R_{\min}}^{R} \frac{r^2}{R - R_{\min}} dr = \frac{R^3 - R_{min}^3}{3(R - R_{min})}. \tag{42}$$

B. CALCULATION OF $\mathbb{E}\left[\frac{1}{d_k^2}\right]$

$$\mathbb{E}\left[\frac{1}{d_k^2}\right] = \int_{R_{\min}}^{R} \frac{1}{r^2} f_d(r) dr = \int_{R_{\min}}^{R} \frac{1}{r^2(R - R_{\min})} dr = \frac{1}{RR_{min}}. \tag{43}$$

C. CALCULATION OF $\mathbb{E}\left[\frac{1}{d_k^4}\right]$

$$\mathbb{E}\left[\frac{1}{d_k^4}\right] = \int_{R_{\min}}^{R} \frac{1}{r^4} f_d(r) dr = \int_{R_{\min}}^{R} \frac{1}{r^4(R - R_{\min})} dr = \frac{R^2 + RR_{min} + R_{min}^2}{3R^3 R_{min}^3}. \tag{44}$$

D. CALCULATION OF $\mathbb{E}\left[\log_2\left(\frac{c}{d_k^2}\right)\right]$

$$\begin{aligned}\mathbb{E}\left[\log_2\left(\frac{c}{d_k^2}\right)\right] &= \int_{R_{min}}^{R} \log_2\left(\frac{c}{r^2}\right) \frac{1}{R - R_{min}} dr \\ &= \frac{\log(c) + \frac{2(R - R_{min} - R\log(R) + R_{min}\log(R_{min}))}{R - R_{min}}}{\log(2)}\end{aligned} \tag{45}$$

APPENDIX D APPROXIMATED DISTRIBUTION OF THE TOTAL POWER GAIN OF THE CHANNEL MATRIX

Lemma 3. *Let $\beta_k = \eta/d_k^2$, where $d_k, \forall k$ are i.i.d. random variables following the uniform distribution with PDF given by $1/(R - R_{min})$, therefore, as the number of served devices increases, the PDF of $Z = \sum_{k=1}^{K} M\beta_k$ can be approximated by the Gamma distribution with parameters $\kappa = \frac{3KRR_{min}}{(R-R_{min})^2}$ and $\theta = \frac{M\eta(R-R_{min})^2}{3R^2R_{min}^2}$, i.e., $\Gamma(\kappa, \theta)$.*

Proof. This is empirically proved by comparing the normalised histogram of Z against the theoretical PDF of a Gamma random variable with the parameters defined earlier.

The parameters κ and θ are found by using the mean and variance statistics of Z, where $\kappa = \frac{\mu_Z^2}{\sigma_Z^2}$ and $\theta = \frac{\sigma_Z^2}{\mu_Z}$. These relations are derived based on the definitions of mean and variance of a Gamma random variable. The mean of Z is given by

$$\begin{aligned}\mu_Z &= M\eta \sum_{k=1}^{K} \mathbb{E}\left[\frac{1}{d_k^2}\right] \\ &= MK\eta\mathbb{E}\left[\frac{1}{d_k^2}\right] \\ &= \frac{MK\eta}{RR_{min}},\end{aligned} \tag{46}$$

where we used the assumption that $d_k, \forall k$ are i.i.d. random variables and the results in Appendix C. Next, the variance of Z is given by

$$\sigma_Z^2 = \mathbb{E}[Z^2] - \mu_Z^2, \tag{47}$$

where

$$\begin{aligned}\mathbb{E}[Z^2] &= M^2K\{\mathbb{E}[\beta^2] + (K-1)\mathbb{E}[\beta_k]^2\} \\ &= M^2\eta^2K\left\{\mathbb{E}\left[\frac{1}{d_k^4}\right] + (K-1)\mathbb{E}\left[\frac{1}{d_k^2}\right]^2\right\} \\ &= M^2\eta^2K\left[\frac{R^2 + RR_{min} + R_{min}^2}{3R^3R_{min}^3} - \frac{(K-1)}{R^2R_{min}^2}\right],\end{aligned} \tag{48}$$

where $\mathbb{E}\left[\frac{1}{d_k^4}\right]$ is calculated in Appendix C. Therefore, plugging (48) into (47) we have

$$\sigma_Z^2 = \frac{K\eta^2M^2(R - R_{min})^2}{3R^3R_{min}^3}. \tag{49}$$

The proof is concluded by replacing (46) and (49) into the definitions of κ and θ.

□

APPENDIX E APPROXIMATED DISTRIBUTION OF THE INSTANTANEOUS SUM-CAPACITY IN HIGH SNR REGIME AND FAVORABLE PROPAGATION

In this appendix we demonstrate how the parameters κ and θ are derived. These parameters, which are used to approximate the instantaneous sum-capacity PDF in high SNR regime and favorable propagation, are found by using the mean and variance statistics of the random variable given by (30), where $\kappa = \frac{\mu_{C_{\text{inst.}}}^2}{\sigma_{C_{\text{inst.}}}^2}$ and $\theta = \frac{\sigma_{C_{\text{inst.}}}^2}{\mu_{C_{\text{inst.}}}}$. These relations are derived based on the definitions of mean and variance of a Gamma random variable. The mean of (30) is given by

$$\begin{aligned}\mu_{C_{\text{inst.}}} &= \mathbb{E}[C_{\text{inst.}}] \\ &= \mathbb{E}\left[\sum_{k=1}^{K} \log_2\left(\frac{\rho M\eta}{d_k^2}\right)\right] \\ &= \sum_{k=1}^{K} \mathbb{E}\left[\log_2\left(\frac{\rho M\eta}{d_k^2}\right)\right] \\ &= K\mathbb{E}\left[\log_2\left(\frac{\rho M\eta}{d_k^2}\right)\right] \\ &= K\frac{\log(\rho M\eta) + \frac{2(R - R_{min} - R\log(R) + R_{min}\log(R_{min}))}{R - R_{min}}}{\log(2)},\end{aligned} \tag{50}$$

where we used the assumption that $d_k, \forall k$ are i.i.d. random variables and the result in Appendix C-D. Next, the variance of (30) is given by

$$\sigma_{C_{\text{inst.}}}^2 = \mathbb{E}[C_{\text{inst.}}^2] - \mathbb{E}[C_{\text{inst.}}]^2, \tag{51}$$

where $\mathbb{E}[C_{\text{inst.}}^2]$ is given by (52) with $\mathbb{E}\left[\log_2^2\left(\frac{\rho M\eta}{d_k^2}\right)\right]$ being defined by (53) with $a = \log(\rho M\eta)$, $b = R - R_{min}$, $c = \log(R)$, $d = \log(R_{min})$. Therefore, plugging (50) and (52) into (51) we have (54). The proof is concluded by replacing (50) and (54) into the definitions of κ and θ.

$$\begin{aligned}\mathbb{E}[C_{\text{inst.}}^2] &= K\left\{\mathbb{E}\left[\log_2^2\left(\frac{\rho M\eta}{d_k^2}\right)\right] + (K-1)\mathbb{E}\left[\log_2\left(\frac{\rho M\eta}{d_k^2}\right)\right]^2\right\} \\ &= K\left\{\mathbb{E}\left[\log_2^2\left(\frac{\rho M\eta}{d_k^2}\right)\right] - \mathbb{E}\left[\log_2\left(\frac{\rho M\eta}{d_k^2}\right)\right]^2\right\} \\ &= \frac{K\left(\frac{a^2b+4a(R-cR-R_{min}+dR_{min})+8b+4cR(c-2)-4d(d-2)R_{min}}{b} - K^2\left(a+\frac{2(R-cR-R_{min}+dR_{min})}{b}\right)^2\right)}{\log^2(2)}.\end{aligned} \tag{52}$$

$$\begin{aligned}\mathbb{E}\left[\log_2^2\left(\frac{\rho M\eta}{d_k^2}\right)\right] &= \int_{R_{min}}^{R}\log_2^2\left(\frac{\rho M\eta}{d_k^2}\right)\frac{1}{R-R_{min}}dr \\ &= \frac{a^2b+4a(R-cR-R_{min}+dR_{min})+8b+4cR(c-2)-4d(d-2)R_{min}}{b\log^2(2)}.\end{aligned} \tag{53}$$

$$\sigma_{C_{\text{inst.}}}^2 = \frac{K\left(\frac{b\log^2(c)+4a(R-cR-R_{min}+dR_{min})+8b+4c(c-2)R-4d(d-2)R_{min}}{b} - K(K+1)\left(a+\frac{2(R-cR-R_{min}+dR_{min})}{b}\right)^2\right)}{\log^2(2)} \tag{54}$$

ACKNOWLEDGMENT

This work was funded by the European Union's Horizon 2020 research and innovation programme under grant agreement No. 732174 (ORCA project). Additionally, this work was partially supported by R&D ANEEL - PROJECT COPEL 2866-0366/2013. This work was partially funded by EMBRAPII - Empresa Brasileira de Pesquisa e Inovacao Industrial. E. R. Lima was supported in part by CNPq under Grant 313239/2017-7. G. Fraidenraich was supported in part by CNPq under Grant 304946/2016-8.

REFERENCES

[1] T. L. Marzetta, Fundamentals of massive MIMO. Cambridge University Press, 2016.

[2] E. Björnson, L. Sanguinetti, H. Wymeersch, J. Hoydis, and T. L. Marzetta, "Massive mimo is a reality—what is next?: Five promising research directions for antenna arrays," Digital Signal Processing, vol. 94, pp. 3 – 20, 2019.

[3] F. A. P. de Figueiredo, F. A. C. M. Cardoso, I. Moerman, and G. Fraidenraich, "On the application of massive mimo systems to machine type communications," IEEE Access, vol. 7, no. 12, pp. 2589–2611, 2018.

[4] K. Haneda, J. Zhang, L. Tan, G. Liu, Y. Zheng, H. Asplund, J. Li, Y. Wang, D. Steer, C. Li, et al., "5G 3GPP-like channel models for outdoor urban microcellular and macrocellular environments," in 2016 IEEE 83rd Vehicular Technology Conference (VTC Spring), pp. 1–7, IEEE, 2016.

[5] Z. Pi, J. Choi, and R. Heath, "Millimeter-wave gigabit broadband evolution toward 5G: Fixed access and backhaul," IEEE Communications Magazine, vol. 54, no. 4, pp. 138–144, 2016.

[6] E. Bjornson, L. Van der Perre, S. Buzzi, and E. G. Larsson, "Massive MIMO in sub-6 GHz and mmWave: Physical, practical, and use-case differences," IEEE Wireless Communications, vol. 26, no. 2, pp. 100–108, 2019.

[7] J. G. Andrews, X. Zhang, G. D. Durgin, and A. K. Gupta, "Are we approaching the fundamental limits of wireless network densification?," IEEE Communications Magazine, vol. 54, pp. 184–190, October 2016.

[8] H. Yang and T. L. Marzetta, "Energy Efficiency of Massive MIMO: Cell-Free vs. Cellular," in 2018 IEEE 87th Vehicular Technology Conference (VTC Spring), pp. 1–5, IEEE, 2018.

[9] S. A. Hassan, M. S. Omar, M. A. Imran, J. Qadir, and D. Jayako, "Universal access in 5G networks, potential challenges and opportunities for urban and rural environments," 5G Networks: Fundamental Requirements, Enabling Technologies, and Operations Management, 2017.

[10] W. K. Pan and R. E. Bilsborrow, "The use of a multilevel statistical model to analyze factors influencing land use: a study of the ecuadorian amazon," Global and Planetary Change, vol. 47, no. 2-4, pp. 232–252, 2005.

[11] L. Gonsioroski, M. C. de Almeida, P. Castellanos, D. Okamoto, J. Arnez, R. Souza, and L. da Silva Mello, "Preliminary results of channel characterization at 700mhz band in urban and rural regions," in 2014 International Telecommunications Symposium (ITS), pp. 1–5, IEEE, 2014.

[12] J. Van Rees, "Measurements of the wide-band radio channel characteristics for rural, residential, and suburban areas," IEEE Transactions on Vehicular Technology, vol. 36, no. 1, pp. 2–6, 1987.

[13] P. Chandhar, D. Danev, and E. G. Larsson, "Massive MIMO as enabler for communications with drone swarms," in 2016 International Conference on Unmanned Aircraft Systems (ICUAS), pp. 347–354, IEEE, 2016.

[14] P. Chandhar, D. Danev, and E. G. Larsson, "On the outage capacity in massive mimo with line-of-sight," in 2017 IEEE 18th International Workshop on Signal Processing Advances in Wireless Communications (SPAWC), pp. 1–6, July 2017.

[15] E. Becirovic, E. Björnson, and E. G. Larsson, "How much will tiny iot nodes profit from massive base station arrays?," in 2018 26th European Signal Processing Conference (EUSIPCO), pp. 832–836, IEEE, 2018.

[16] P. Chandhar and E. G. Larsson, "Massive mimo for connectivity with drones: Case studies and future directions," IEEE Access, vol. 7, pp. 94676–94691, 2019.

[17] P. Chandhar, D. Danev, and E. G. Larsson, "On the zero-forcing receiver performance for massive MIMO drone communications," in 2018 IEEE 19th International Workshop on Signal Processing Advances in Wireless Communications (SPAWC), pp. 1–5, IEEE, 2018.

[18] A. Garcia-Rodriguez, G. Geraci, D. López-Pérez, L. G. Giordano, M. Ding, and E. Björnson, "The Essential Guide to Realizing 5G-Connected UAVs with Massive MIMO," arXiv preprint arXiv:1805.05654, 2018.

[19] Y. Hu, Y. Hong, and J. Evans, "Interference in los massive mimo is well approximated by a beta-mixture," in 2015 IEEE International Conference on Communication Workshop (ICCW), pp. 1137–1142, June 2015.

[20] C. Feng, Y. Jing, and S. Jin, "Interference and outage probability analysis for massive mimo downlink with mf precoding," IEEE Signal Processing Letters, vol. 23, pp. 366–370, March 2016.

[21] H. Q. Ngo, E. G. Larsson, and T. L. Marzetta, "Aspects of favorable propagation in massive MIMO," in 2014 22nd European Signal Processing Conference (EUSIPCO), pp. 76–80, IEEE, 2014.

[22] T. Hälsig and B. Lankl, "Array size reduction for high-rank los mimo ulas," IEEE Wireless Communications Letters, vol. 4, pp. 649–652, Dec 2015.

[23] P. Chandhar, D. Danev, and E. G. Larsson, "On ergodic rates and optimal array geometry in line-of-sight massive MIMO," in 2016 IEEE 17th International Workshop on Signal Processing Advances in Wireless Communications (SPAWC), pp. 1–6, IEEE, 2016.
[24] C. A. Balanis, Antenna Theory: Analysis and Design. Wiley Interscience, 2005.
[25] D. Tse and P. Viswanath, Fundamentals of Wireless Communication. New York, NY, USA: Cambridge University Press, 2005.
[26] H. Q. Ngo, E. G. Larsson, and T. L. Marzetta, "Energy and Spectral Efficiency of Very Large Multiuser MIMO Systems," IEEE Transactions on Communications, vol. 61, pp. 1436–1449, April 2013.
[27] A. L. Giuseppa Alfano and S. Verdu, "Mutual Information and Eigenvalue Distribution of MIMO Ricean Channels," in International Symposium on Information Theory and its Applications (ISITA2004), 2004.
[28] Z. Chen and E. Björnson, "Channel hardening and favorable propagation in cell-free massive MIMO with stochastic geometry," IEEE Transactions on Communications, vol. 66, no. 11, pp. 5205–5219, 2018.
[29] J. H. Emil Bjornson and L. Sanguinetti, Massive MIMO Networks: Spectral, Energy, and Hardware Efficiency. Now Publishers, 2017.
[30] Wolfram Research, "Mathematica," 2018.
[31] T. M. Cover and J. A. Thomas, Elements of Information Theory (Wiley Series in Telecommunications and Signal Processing). New York, NY, USA: Wiley-Interscience, 2006.
[32] R. A. Horn and C. R. Johnson, Matrix Analysis. New York, NY, USA: Cambridge University Press, 2nd ed., 2012.